Progress In Electromagnetics Research Letters, Vol. 74, 23–30, 2018

Design of a Dual-Band MIMO Antenna with High Isolation for WLAN Applications

Peng Liu, Deming Sun, Peng Wang*, and Peng Gao

Abstract—A dual-band two-element Multiple-Input-Multiple-Output (MIMO) antenna for Wireless Local Area Network (WLAN) applications is proposed in this paper. The MIMO antenna consists of two closely arranged symmetric monopole antennas with edge-to-edge distance of only 5.3 mm (0.044λ at 2.51 GHz). To enhance isolation, a decoupling network is inserted between the two antennas without increasing the footprint. The -10 dB impedance bandwidths in lower and higher frequency bands are 2.46–2.7 GHz and 5.04–5.5 GHz. Compared to previous works, the presented decoupling structure can obtain higher isolation over 30 dB in dual bands. Measured results agree well with the simulated ones.

1. INTRODUCTION

Wireless local area networks (WLANs) have attracted tremendous attention due to the demand of higher speed connectivity and better data reliability with rapid development of wireless communication systems [1, 2]. Multiple-input-multiple-output (MIMO) systems characterized by multipath property are widely used to increase system capacity and communication reliability. However, when antenna elements are implemented in a size-constraint space, it is a challenging issue to obtain high isolation due to considerable electromagnetic mutual coupling between ports.

In the literature, various decoupling techniques have been proposed to resolve the issue. Defected ground structures [3–5] act as band stop filters to achieve high isolation by inhibiting surface waves. Neutralization lines [6–8] are employed to offset the original coupling through introducing extra coupling path. Parasitic elements [9, 10] are embedded between antenna elements to introduce extra coupling paths to enhance isolation. Lumped network [11] and resonator decoupling network [12] are applied to increase isolation. A Y-shaped isolator [13] is introduced to decrease mutual coupling between dual-element antennas. In [14], a split ring decoupling structure realizing hybrid electric and magnetic coupling is adopted for isolation enhancement. Nevertheless, isolation levels achieved in antennas mentioned above are 20 dB more or less, which is insufficient in certain application situations. Moreover, the distance between antenna elements described in these aforementioned designs is more than 0.05λ, which affects the miniaturization of a MIMO antenna. Although some MIMO antennas mentioned above have compact size, the isolation levels or bandwidths are insufficient in certain applications, and it is unfeasible to obtain isolation over 30 dB between two closely arranged antennas with less than 0.05λ separation distance.

In this letter, the proposed MIMO antenna consists of two symmetrical antenna elements arranged with edge-to-edge distance of 5.3 mm (0.044λ at 2.51 GHz), which is the smallest among those dual-band MIMO antennas [5, 13, 15–17]. The decoupling structure in this paper constructs an extra coupling path to offset the original coupling. Thus, the coupling current is canceled out by the new current in the extra coupling path, and high isolation over 30 dB is easily realized. The MIMO system performances, including S-parameters, radiation patterns, current distribution, gains and radiation efficiency, are investigated and presented.

Received 10 January 2018, Accepted 28 February 2018, Scheduled 9 March 2018

* Corresponding author: Peng Wang (wangpeng@uestc.edu.cn).

The authors are with the Research Institute of Electronic Science and Technology, Information Geoscience Research Center, University of Electronic Science, and Technology of China Chengdu, China.

2. ANTENNA DESIGN

Figure 1(a) exhibits geometry of the proposed two-element dual-band MIMO antenna. The antenna is designed using full-wave simulator Ansoft HFSS 13.0 and implemented on a 1.6-mm-thick FR-4 substrate of relative permittivity of 4.4 and loss tangent of 0.02. Feeding ports are coaxial through via holes of 0.7 mm radius. The MIMO antenna is composed of two symmetric monopole antenna elements printed on the upper part of a PCB board and a simple decoupling structure for isolation enhancement. The detailed dimensions of the antenna are listed in Table 1.

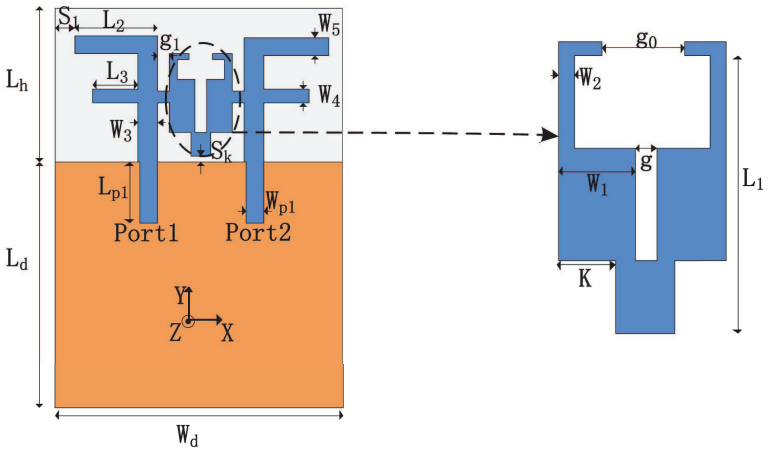

Figure 1. Geometry of the proposed MIMO antenna.

Table 1. Design parameters (mm) of the proposed MIMO antenna.

L_d	W_d	L_h	L_{p1}	W_{p1}	L_1	L_2	L_3	g	g_0
55	47.3	19	8	2.7	12.8	15	5.5	0.3	1.4
g_1	W_1	W_2	W_3	W_4	W_5	S_k	K	S_1	—
0.5	2	0.5	3.5	2.5	3.5	0.2	1.25	6	—

2.1. Design Process of the Proposed MIMO Antenna

The two-element dual-band MIMO antenna in Fig. 2(a) designated as Ant.a is originated by arranging two adjacent monopole antennas with close edge-to-edge distance of only 5.3 mm (0.044λ at 2.51 GHz). The short arm of dimension $L_3 \times W_4$ contributes to the upper resonant frequency at 5.21 GHz while the longer inverted L-shaped arm resonates at 2.3 GHz. Two required bands can be controlled by varying dimensions of two monopole arms. The simulated S-parameters of Ant.a are presented in Fig. 2(c). The two working bands ($|S_{11}| \leq -10$ dB) of Ant.a are received within 2.1–2.58 and 5–5.42 GHz. Meanwhile, Fig. 2(c) shows that the minimum isolations of the two operating bands are -8 and -31 dB, respectively. Hence, isolation and return loss should be optimized to realize better antenna performance.

To maintain the property of compact edge-to-edge distance between two monopole antennas and dimensions of two elements unchanged, a decoupling structure is directly connected to the adjacent monopole [Ant.b, Fig. 2(b)]. After exploiting decoupling structure, simulated S-parameters of Ant.b are shown in Fig. 2(c), which presents that minimum isolation of dual bands is significantly enhanced from 8 dB and 31 dB to 33 dB and 36 dB, respectively. Meanwhile, the lower resonant frequency changes from 2.3 to 2.51 GHz, and the upper resonant frequency is nearly unchanged. The specific effect of the electronic and magnetic coupling structure on the MIMO performance is illustrated in following section.

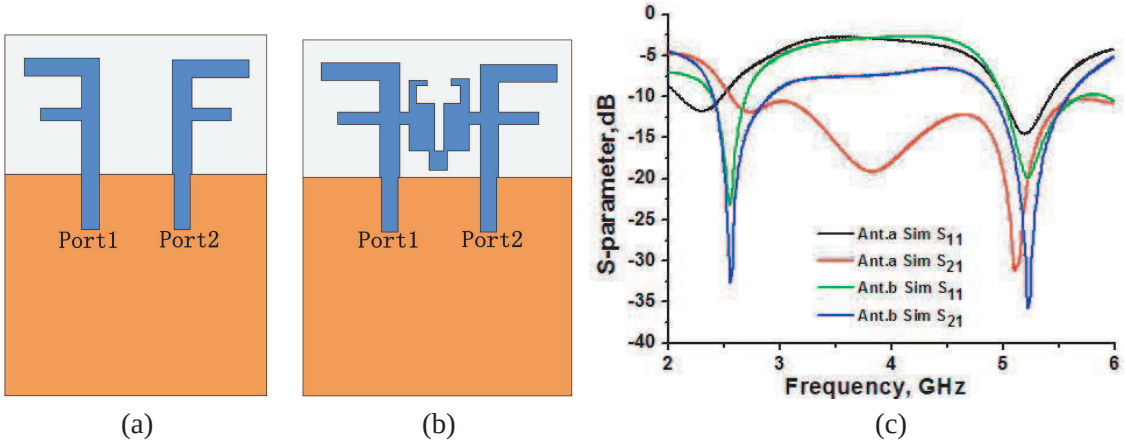

Figure 2. (a) Ant.a and (b) Ant.b and (c) simulated S-parameters of Ant.a and Ant.b.

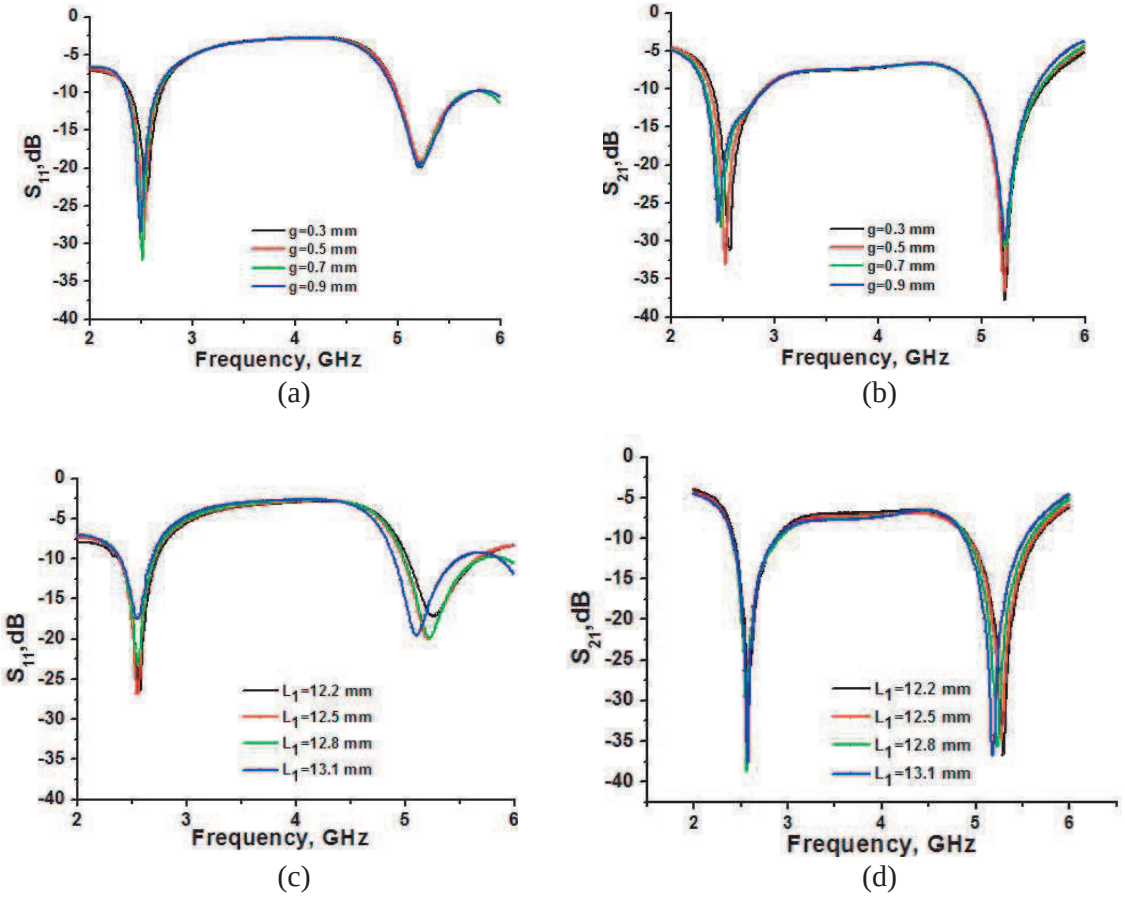

Figure 3. Effect of the width g on (a) S_{11} and (b) S_{21}; and effect of the length L_1 on (c) S_{11} and (d) S_{21}.

2.2. The Effect of Decoupling Structure

There are two important parameters for the decoupling structure in Fig. 1, including width g and length L_1. The effects of width g and length L_1 on S-parameters are analyzed in Fig. 3. It is observed that the isolation is achieved over 30 dB in both resonance frequencies after employing decoupling structure. Meanwhile, the structure also affects the resonant frequencies of dual bands. The results of varying

width g are presented in Figs. 3(a) and (b). For smaller values of width g, the resonance shifts to higher frequencies in the lower band. In the parametric study, length L_1 is a constant. As observed, the resonance of higher band is unaffected for varying values of g. Meanwhile, high isolation over 30 dB is achieved at the lower band due to the original coupling. Finally, width g is optimized at 0.3 mm to obtain the optimal radiating band of 2.51 GHz. Then, parametric analysis of length L_1 is evaluated. The width is kept constant, and length L_1 varies from 12.2 to 13.1 mm. The analysis results are shown in Figs. 3(c) and (d). It is indicated that resonance shifts to lower frequency for larger values of length L_1 in upper band, and resonance of lower band is slightly affected for various lengths L_1. Meanwhile, isolation is little affected. Finally, length L_1 is optimized at 12.8 mm to achieve the optimal radiating band of 5.21 GHz.

To further demonstrate the contribution of the decoupling structure, the current distributions of Ant.a and Ant.b in the two resonant frequency bands are plotted in Figs. 4 and 5, respectively. Figs. 4 and 5 show that the induced current at port 2 before decoupling is strong at 2.51 GHz while it is weak at 5.21 GHz. The performance corresponds to the results shown in Fig. 2(c), in which the isolation is lower than 10 dB and higher than 30 dB at the lower and upper frequency bands, respectively. In Fig. 4(a), strong electromagnetic energy coupling occurs between two antenna elements due to ground

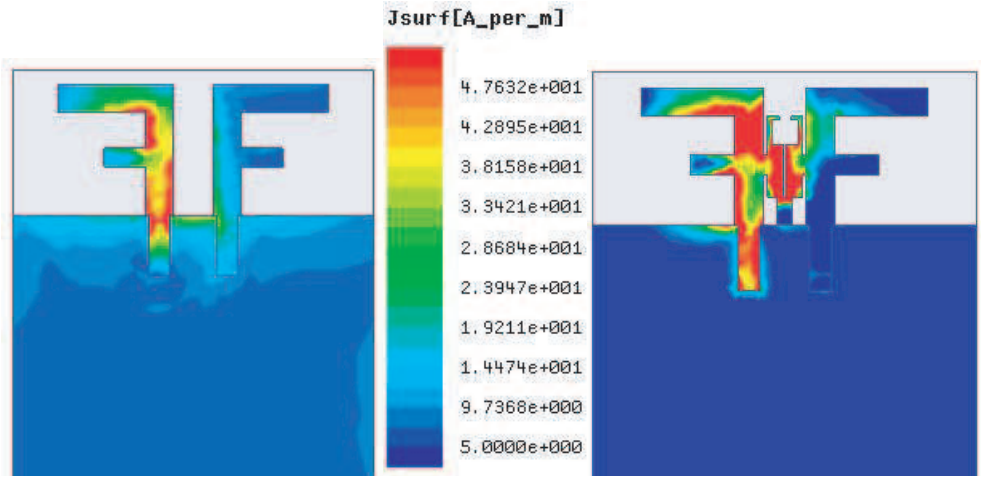

Figure 4. Current distribution of (a) Ant.a and (b) Ant.b at 2.51 GHz.

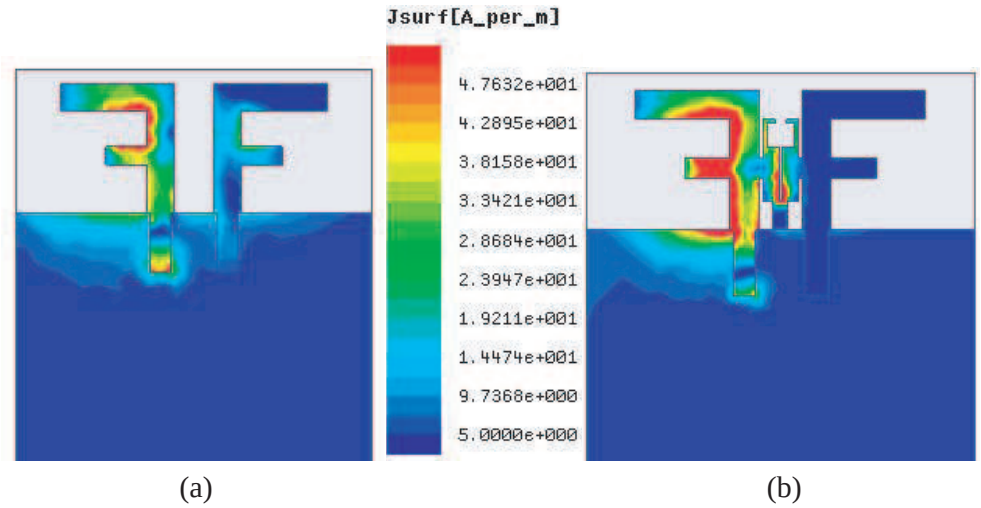

Figure 5. Current distribution of (a) Ant.a and (b) Ant.b at 5.21 GHz.

surface and near-field current at 2.51 GHz, which accounts for poor isolation of 8 dB. Fig. 5(b) reveals that the decoupling structure provides an extra path for coupling fields to introduce new current in opposite phase between two elements. Hence, mutual electric and magnetic coupling between two ports is obviously compensated for the new coupling introduced through the decoupling structure at 2.51 GHz. Finally, a negligible amount of electromagnetic energy is coupled from port 1 to port 2. Fig. 5 presents the current distributions of Ant.a and Ant.b at 5.21 GHz. Fig. 5(a) shows that a small amount of current is coupled from port 1 to port 2 before decoupling. Therefore, good isolation of 31 dB is realized in Ant.a at 5.21 GHz. After using decoupling structure, there are almost no current coupled from port 1 to port 2 shown in Fig. 5(b). Therefore, enough isolation of 36 dB is achieved at 5.21 GHz.

3. RESULTS AND DISCUSSION

A prototype of the proposed dual-band MIMO antenna shown in Fig. 6 is fabricated, and the simulated and measured S-parameters are plotted in Fig. 7. The S-parameters are measured through an Agilent E8363B vector network analyzer. As shown in Fig. 7, measured results correspond well to the simulated data. The -10 dB impedance bandwidths at lower and upper bands are 2.46–2.7 GHz and 5.04–5.5 GHz, with fractional bandwidths of 9.6% and 8.84%, respectively. Meanwhile, the measured value of minimum port isolation in the two operating bands is over 30 dB.

The simulated and measured normalized radiation patterns of the dual-band MIMO antenna are shown in Fig. 8, when port 1 is excited and port 2 terminated by a matched load. Good agreement is presented between the simulated and measured results. The antenna is nearly omnidirectional at XZ and YZ planes in both operating bands. Fig. 9 shows that the simulated peak gains of 2.51 GHz

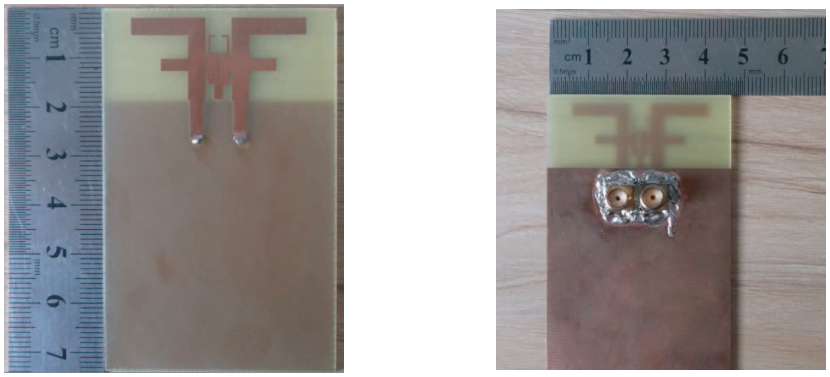

Figure 6. Photograph of the proposed MIMO antenna, (a) top view and (b) back view.

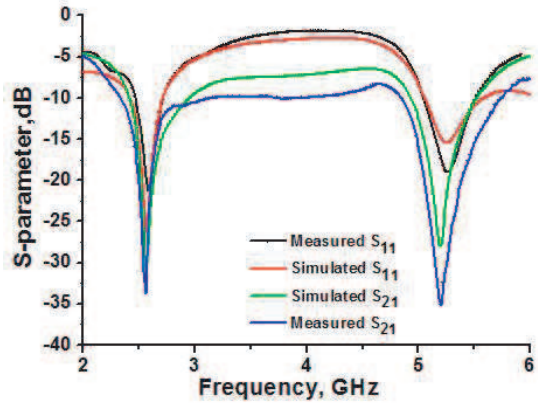

Figure 7. Simulated and measured S-parameters of the designed MIMO antenna.

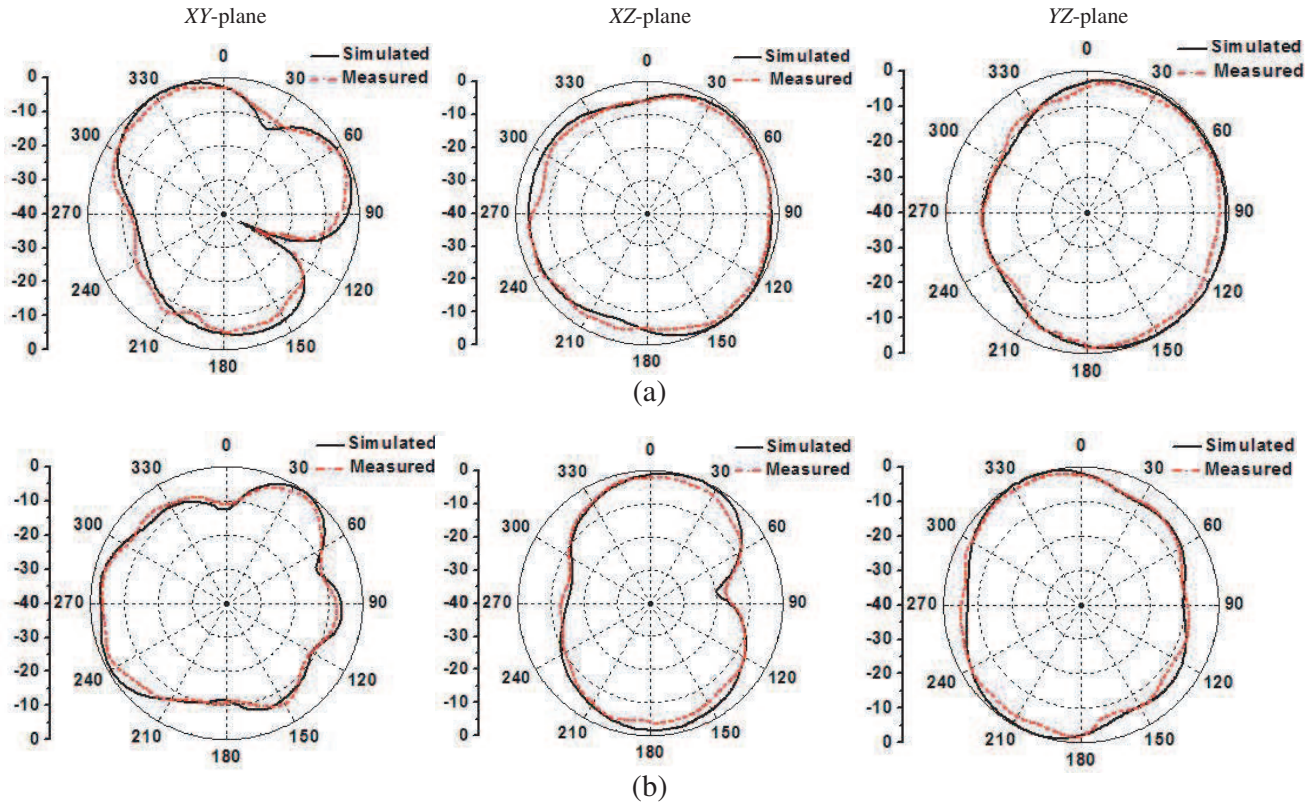

Figure 8. Simulated and measured normalized radiation patterns, (a) 2.51 GHz and (b) 5.21 GHz.

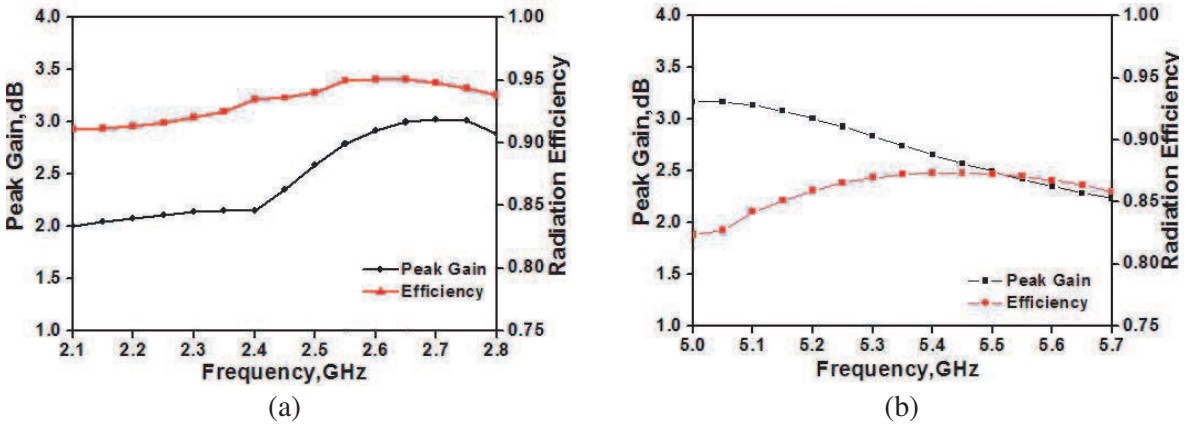

Figure 9. Simulated peak gain and total efficiency, (a) lower band and (b) upper band.

and 5.21 GHz are 2.59 and 3 dBi, respectively. Next, the simulated total efficiency of the antenna is plotted in Fig. 8. The simulated average efficiencies are 93.3% and 85.9% in the lower and upper bands, respectively. Diversity performance of a MIMO antenna can be investigated by computing envelope correlation coefficient (ECC). The ECC is calculated from far-field radiation patterns [18]. As seen in Fig. 10, ECC of the MIMO antenna is below 0.01 in the two frequency bands, and it is indicated that a good diversity performance of the MIMO antenna can be realized. The designed antenna is compared with some dual-band MIMO antennas in previous works, as seen in Table 2. It is observed that the antenna can obtain both 20 and 30 dB isolation bandwidths compared to others with a very small edge-to-edge distance.

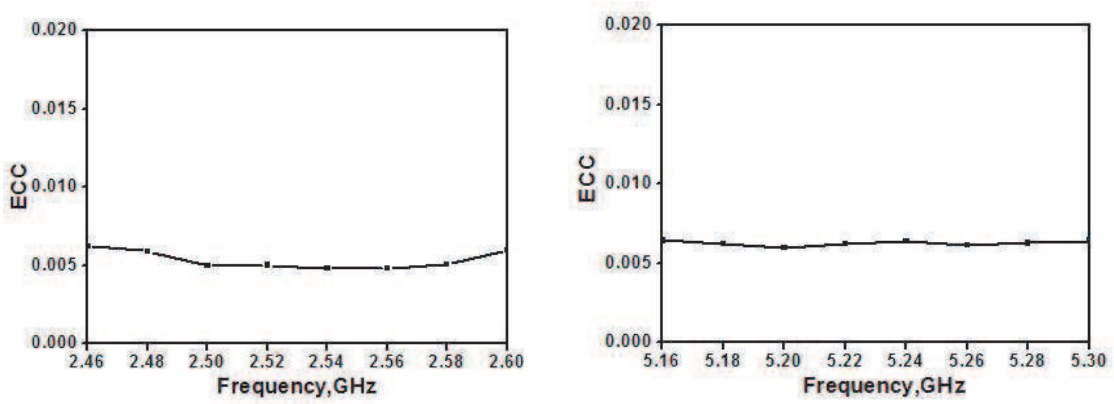

Figure 10. Calculated ECC of the proposed antenna.

Table 2. Performance comparison with some previous works.

Ref.	Operating frequency f_1/f_2 (GHz)	Edge-to-edge distance (mm)	20 dB isolation Bandwidth (%)		30 dB isolation Bandwidth (%)	
			Lower band	Upper band	Lower band	Upper band
[3]	2.5/5.6	6 ($0.05\lambda_1$)	10.8	3.2	—	—
[11]	2.45/5.5	8.5 ($0.069\lambda_1$)	4.08	—	—	—
[13]	0.82/2.65	15 ($0.041\lambda_1$)	1.59	3.02	1	—
[14]	2.44/5.5	22.4 ($0.182\lambda_1$)	—	10	—	—
[15]	2/5.5	30 ($0.2\lambda_1$)	16	5.4	2.5	—
This work	2.51/5.21	5.3 ($0.044\lambda_1$)	7.2	7.3	4	3.85

*: The isolation bandwidth is calculated under the requirement of $S_{11} \leq -10$ dB.

4. CONCLUSION

In this paper, a dual-band MIMO antenna composed of two closely arranged symmetric monopole antennas with edge-to-edge distance of only 5.3 mm (0.044λ at 2.51 GHz) is proposed for WLAN applications. The operating frequency bands ($|S_{11}| \leq -10$ dB) are 2.46–2.7 and 5.04–5.5 GHz. In the two operating frequency bands, good isolation of over 30 dB is realized considering the antennas' sub-0.1λ separation. Moreover, the measured results agree well with the simulated ones, which confirms that the proposed antenna can be a potential candidate for wireless local area network applications in practical devices.

REFERENCES

1. Palandoken, M., "Dual broadband antenna with compact double ring radiators for IEEE 802.11 ac/b/g/n WLAN communication applications," *Turkish Journal of Electrical Engineering & Computer Sciences*, Vol. 25, 1326–1333, DOI: 10.3906/elk-1507-121, 2016.
2. Palandoken, M., "Artificial materials based microstrip antenna design," *Microstrip Antennas*, InTech, ISBN: 978-953-307-247-0, 2011.
3. Li, J. F., Q. X. Chu, and T. G. Huang, "A compact wideband MIMO antenna with two novel bent slits," *IEEE Trans. Antennas Propag.*, Vol. 2, No. 60, 482–489, 2012.
4. Chiu, C. Y., C. H. Cheng, R. D. Murch, and C. R. Rowell, "Reduction of mutual coupling between closely-packed antenna elements," *IEEE Trans. Antennas Propag.*, Vol. 55, No. 6, 1732–1738, Jun. 2007.

5. Nandi, S. and A. Mohan, "A compact dual-band MIMO slot antenna for WLAN applications," *IEEE Antennas Wirel. Propag. Lett.*, Vol. 16, 2457–2460, 2017.
6. Su, S. W., C. T. Lee, and F. S. Chang, "Printed MIMO-antenna systems using neutralization-line technique for wireless USB-dongle applications," *IEEE Trans. Antennas Propag.*, Vol. 60, No. 2, 456–463, 2012.
7. Wang, Y. and Z.-W. Du, "A wideband printed dual-antenna with three neutralization lines for mobile terminals," *IEEE Trans. Antennas Propag.*, Vol. 62, No. 3, 1495–1499, Mar. 2014.
8. Ling, X. and R. Li, "A novel dual-band MIMO antenna array with low mutual coupling for portable wireless devices," *IEEE Antennas Wireless Propag. Lett.*, Vol. 10, 1039–1042, 2011.
9. Mak, A. C. K., C. R. Rowell, and R. D. Murch, "Isolation enhancement between two closely packed antennas," *IEEE Trans. Antennas Propag.*, Vol. 56, No. 11, 3411–3419, Nov. 2008.
10. Lau, B. K. and J. B. Andersen, "Simple and efficient decoupling of compact arrays with parasitic scatterers," *IEEE Trans. Antennas Propag.*, Vol. 60, No. 2, 464–472, Feb. 2012.
11. Li, R. P., P. Wang, Q. Zheng, and R. Z. Wu, "Compact microstrip decoupling and matching network for two symmetric antennas," *Electron. Lett.*, Vol. 51, No. 18, 1396–1398, 2015.
12. Zhao, L., L. K. Yeung, and K.-L. Wu, "A coupled resonator decoupling network for two-element compact antenna arrays in mobile terminals," *IEEE Trans. Antennas Propag.*, Vol. 62, No. 5, 482–289, 2014.
13. Khan, M. S., M. F. Shafique, A. Naqvi, A. D. Capobianco, B. Ijaz, and B. D. Braaten, "A miniaturized dual-band diversity antenna for WLAN applications," *IEEE Antennas Wirel. Propag. Lett.*, Vol. 14, 958–961, 2015.
14. Xue, C.-D., X.-Y. Zhang, Y.-F. Cao, Z.-J. Hou, and C.-F. Ding, "MIMO antenna using hybrid electric and magnetic coupling for isolation enhancement," *IEEE Trans. Antennas Propag.*, Vol. 65, No. 10, 5162–5170, 2017.
15. Sharawi, M.-S., A.-B. Numan, M.-U. Khan, and D.-N. Aloi, "A dual-element dual-band MIMO antenna system with enhanced isolation for mobile terminals," *IEEE Antennas Wirel. Propag. Lett.*, Vol. 11, 1006–1009, 2012.
16. Li, Q. L., S. W. Cheung, D. Wu, and T. I. Yuk, "Optically transparent dual-band MIMO antenna using micro-metal mesh conductive film for WLAN system," *IEEE Antennas Wirel. Propag. Lett.*, Vol. 16, 920–923, 2017.
17. Cheung, S.-W., Q.-L. Li, D. Wu, C.-F. Zhou, and B. Wang, "Defected ground structure with two resonances for decoupling of dual-band MIMO antenna," *IEEE International Symposium on AP-S&/USNC/URSI*, 1645–1646, 2017.
18. Khan, M. S., M. F. Shafique, A. D. Capobianco, E. Autizi, I. Shoaib, and I. Ali, "Compact UWB-MIMO antenna array with a floating digitated decoupling structure," *IET Microwaves, Antennas & Propagation*, Vol. 8, No. 10, 747–753, Mar. 2014.